Stable Copper−Tin Cluster Compositions from High-Temperature Annealing

Gary A. Breaux, Damon A. Hillman, Colleen M. Neal, and Martin F. Jarrold*

Department of Chemistry, Indiana University, 800 E. Kirkwood Avenue, Bloomington, Indiana 47404

Received: January 10, 2005; In Final Form: July 8, 2005

Copper-doped tin clusters can be thermally annealed to much more stable compositions with a substantially higher copper/tin ratio. The annealed clusters are only prominent over a narrow range of compositions: $CuSn_{10-15}^+$, $Cu_2Sn_{12-18}^+$, $Cu_3Sn_{15-21}^+$, $Cu_4Sn_{18-(24)}^+$, and $Cu_5Sn_{21-(27)}^+$. These compositions are close to those found for $W_mSi_n^+$ clusters, raising the possibility that the $Cu_mSn_n^+$ clusters have core−shell geometries like those proposed for the $W_mSi_n^+$ clusters. Increasing the number of copper atoms causes a change in the dissociation pattern from the fission processes that are characteristic of semiconductor clusters to the expulsion of individual atoms, which usually occurs for metal clusters. The change in the fragmentation pattern may result because the clusters rich in copper melt before they dissociate, while the pure tin clusters dissociate directly from a solidlike phase.

Introduction

Metal encapsulated silicon and germanium clusters have received a lot of attention recently because of their potential for generating cluster assembled materials with tunable electronic, optical, and magnetic properties. Calculations suggest that small silicon and germanium clusters can be stabilized by encapsulating a metal atom, and a wide variety of metal guests have been examined.[1−21] The experimental evidence for cage structures is often indirect. Beck, the first to study mixed metal−silicon clusters, generated them by seeding metal carbonyls into the helium flow of a laser vaporization source and found prominent peaks for MSi_n^+ with $n = 15$ and 16 and M = W, Mo, and Cr.[22,23] He found that the metal atom stabilized the clusters against photodissociation and suggested that it could act as a "seed" for silicon atoms to condense upon. More recently, Kaya and co-workers used a laser vaporization source with two target rods (silicon and a metal) to produce MSi_n^+ for M = Ti, Hf, Mo, W, and Tb and studied them using mass spectrometry, a chemical probe (water adsorption), and photoelectron spectroscopy.[24,25] They concluded that the metal atom was encapsulated in a silicon cage for $n \geq 15$.

Some of the most convincing experimental evidence for cage structures comes from studies of metal ion reactions with silane. Ohanssian and collaborators found that W^+ reacts with silane to undergo a series of association and dehydrogenation reactions which, they suggested, terminate when the metal gets trapped inside a silicon cage.[26] Kanayama and co-workers[27,28] reacted metal ions (M^+) and metal cluster ions (M_m^+) with silane in an ion trap. The metal ion reactions terminated at MSi_n^+ with $n =$ 14, 13, 12, 11, and 9 for M = Hf, Ta, W, Re, and Ir, respectively. The number of silicon atoms in the terminal products is consistent with the 18-electron rule, which suggests that the stability of the cage is at least partly influenced by electronic factors. The reactions of the W_n^+ clusters ($n = 1-5$) with silane terminate at $W_mSi_n^+$ $n = 12$ for $m = 1$; $n = 17-18$ for $m = 2$; $n = 22$ for $m = 3$; $n = 25-26$ for $m = 4$; and $n =$ 29 for $m = 5$. This pattern is consistent with the formation of cage structures by close packing around a metal center.

Although bulk tin is a metal at room temperature and pressure, in the nanometer size regime tin behaves very much like silicon and germanium. Small tin clusters have geometries that are closely related to those of their silicon and germanium analogues.[29−34] Here, we report studies of copper-doped tin clusters prepared by laser vaporization of a liquid, mixed-metal target. We find that, when they are annealed at high temperature, the copper-doped tin clusters convert (by incorporating more copper atoms) into more stable compositions that are substantially richer in copper. The annealed clusters are only prominent over a narrow range of compositions: $CuSn_{10-15}^+$, $Cu_2Sn_{12-18}^+$, $Cu_3Sn_{15-21}^+$, $Cu_4Sn_{18-(24)}^+$, and $Cu_5Sn_{21-(27)}^+$. The compositions observed here are similar to those found for the $W_mSi_n^+$ clusters mentioned above.

Experimental Methods

The experimental apparatus has been described in detail previously.[35] The cluster ions are created by laser vaporization of a liquid metal target (either pure tin or tin with around 1% copper). We use a liquid metal target, because it provides more stable cluster signals than solid targets. In the present case, it also allows us to easily prepare binary targets. The copper−tin targets were prepared by melting roughly equal amounts of copper and tin with a hydrogen/oxygen torch and then adding more tin to the melt to make a homogeneous sample of around 99% tin and 1% copper. The source, except for the liquid metal target holder, is held at 253 K. A flow of helium buffer gas sweeps the clusters out of the source and carries them into a 10-cm-long, 2.5-mm internal diameter, temperature-variable extension which can be adjusted between 77 and 1073 K. Ions that exit the extension are focused into the first quadrupole mass spectrometer, which can be used to select a specific cluster or can be set to transmit all ions above a threshold mass. At the end of the quadrupole, the ions are focused into the collision cell which is operated with 1 Torr of helium. Under these conditions, the ions undergo many relatively gentle collisions with the helium collision gas, where only a small fraction of the ions' translational energy is converted into internal energy (around 0.012), because the collision partner (helium) is so light.[36] Intact parent ions and fragment ions are swept across the collision cell by a small voltage, and some of them exit through a 1-mm-diameter aperture. The ions that exit are focused

10.1021/jp0501650 CCC: $30.25
Published on Web 09/14/2005

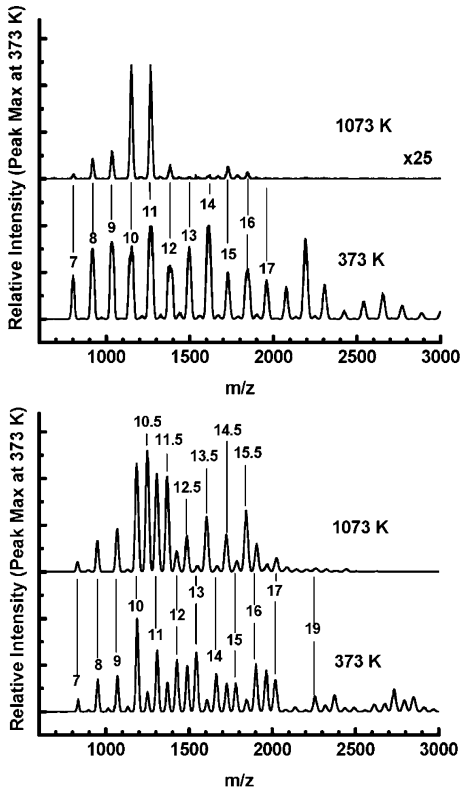

Figure 1. Mass spectra measured with the extension temperatures at 373 and 1073 K for tin clusters (upper spectra) and copper tin clusters (lower spectra). The injection energy was 150 eV. The peaks in the mass spectra have either integer or half-integer labels corresponding to the number of tin atoms in a cluster with a similar nominal mass.

into the second quadrupole mass spectrometer where they are analyzed and then detected. The translational energy with which the ions enter the collision cell is determined from the voltage difference between the source extension and the collision cell.

Results

The upper half of Figure 1 shows mass spectra recorded for pure tin clusters with the source extension set to 373 and 1073 K. These spectra were recorded by scanning the second quadrupole with the first one set to the transmit-all-ions mode. For the spectra shown in Figure 1, the ions were injected into the collision cell with a translational energy of 150 eV. This is sufficiently low that dissociation in the collision cell does not significantly perturb the results. The spectrum at 373 K shows a robust distribution of cluster ions extending to beyond Sn_{25}^+. As the temperature is raised, the larger clusters disappear and the distribution moves to smaller sizes. First, Sn_{19}^+ emerges as a prominent peak and then entirely disappears at around 773 K, then Sn_{15}^+ becomes a prominent peak. At 1073 K, only Sn_{10}^+ and Sn_{11}^+ remain in significant abundance, and the intensity of these peaks is very much reduced from their intensity at 373 K (note the 25× scale change).

The lower half of Figure 1 shows mass spectra recorded with a liquid metal target of around 99% tin and 1% copper. The spectrum is complicated, indeed even more so than it initially appears, because the mass of a copper atom is roughly half the mass of a tin atom, and because both tin and copper have isotope distributions that make it impossible to resolve peaks due to $Cu_mSn_n^+$ from those due to $Cu_{m+2}Sn_{n-1}^+$, at least with a quadrupole mass spectrometer. This is illustrated in Figure 2, which shows calculated isotope profiles for Sn_{17}^+ and $Cu_2Sn_{16}^+$. The mass difference between $Cu_mSn_n^+$ and $Cu_{m+2}Sn_{n-1}^+$ is 8.38

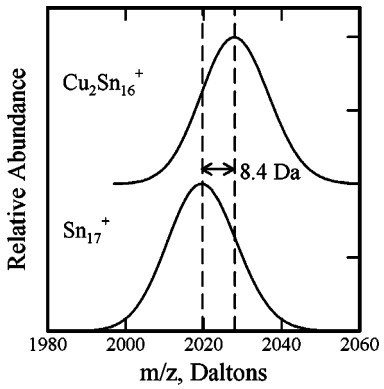

Figure 2. Calculated isotope profiles for Sn_{17}^+ and $Cu_2Sn_{16}^+$. These clusters have such broad isotope profiles that they cannot be resolved. However, there is a significant shift in the position of the peaks which can be monitored (see text).

daltons, and we show below that the shift in the position of the peaks can be used to determine the composition of the clusters, even if the peaks themselves cannot be resolved. Another way to examine the composition of the clusters is to separate them and fragment them. Thus, if we isolate the Sn_n^+ clusters with the source extension at 373 K, they fragment entirely like the Sn_n^+ clusters generated from a pure tin target.

Because a copper atom has roughly half the mass of a tin atom, we find it convenient to label the peaks in the mass spectrum with either integer or half-integer labels corresponding to the number of tin atoms in a cluster with a similar nominal mass. Thus, for example, the label 15 corresponds to Sn_{15}^+ (and $Cu_2Sn_{14}^+$) and the label 15.5 corresponds to $CuSn_{15}^+$ (and $Cu_3Sn_{14}^+$). With the source extension at 373 K, both the position of the 15.5 peak and its fragmentation pattern are consistent with the presence of only a single copper atom. This is true for all of the half-integer peaks present at 373 K, so with the extension set close to room temperature, the clusters present are predominantly Sn_n^+ and $CuSn_n^+$. Note in Figure 1 the abrupt increase in the intensities of the half-integer peaks at 10.5, which corresponds to $CuSn_{10}^+$. It is interesting to note that Beck found the silicon analogue, $CuSi_{10}^+$, to be particularly prominent in his early studies of metal-doped silicon clusters.[21]

More clusters survive at the higher temperature for the mixed copper−tin clusters than survive for the pure tin clusters (see Figure 1). However, in most cases, the peaks in the copper−tin spectra have shifted significantly from their positions at 373 K, indicating an increase in the number of copper atoms present. This is demonstrated in Figure 3, which shows plots of the shift in the integer and half-integer peak positions at 1073 K. For the integer peaks, the shifts are relative to the positions of the Sn_n^+ clusters, and the half-integer peaks are relative to the positions of the Sn_nCu^+ clusters. It is evident from this plot that there are steps in the number of copper atoms present at around $Cu_2Sn_{12}^+$, $Cu_3Sn_{15}^+$, $Cu_4Sn_{18}^+$, and $Cu_5Sn_{21}^+$. The steps occur every three tin atoms.

Table 2 shows a summary of the fragmentation products observed in the dissociation of the $Cu_mSn_n^+$ clusters and the temperature range (of the extension) over which they were observed. The pure tin clusters studied here dissociate to generate "fission" products where clusters with 6, 7, 10, and 11 atoms are prominent products, for example

$$Sn_{18}^+ \rightarrow Sn_{11}^+ + Sn_7$$

These dissociation pathways are similar to those observed by Tai and co-workers[32] who performed fragmentation studies of

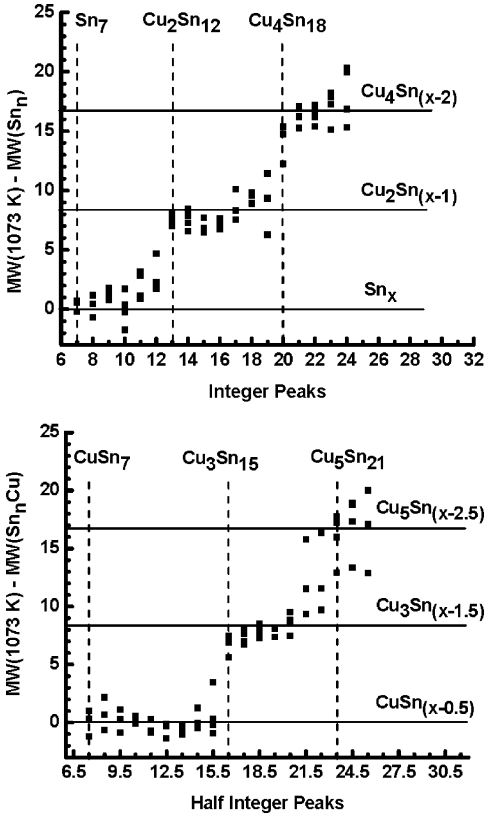

Figure 3. Shift in the peak positions at 1073 K from the mass of the corresponding Sn_n^+ cluster (upper) or $CuSn_n^+$ cluster (lower). The horizontal lines indicate the shifts expected for the substitution of two copper atoms for one tin atom and for substitution of four copper atoms for two tin atoms. The spectra used to generate this plot were recorded with injection energies of 100−250 eV.

TABLE 1: Ranges over Which the $Cu_mSn_n^+$ Clusters with Particular *n* and *m* Values Are Prominent in the Mass Spectra

	m				
n	1	2	3	4	5
	$Cu_mSn_n^+$				
10	X				
11	X				
12	X	X			
13	X	X			
14	X	X			
15	X	X	X		
16		X	X		
17		X	X		
18		X	X	X	
19			X	X	
20			X	X	
21			X	X	X
22				X	X

tin clusters, Sn_n^+ ($n = 4-20$), by low-energy collisions with highly oriented pyrolytic graphite. Metal clusters usually dissociate by sequential evaporation of individual atoms. The fission processes observed with tin clusters are similar to those observed with silicon and germanium clusters. A consideration of the relative energies of the different dissociation pathways, using stabilities derived from density functional theory, shows that the tin cluster fragmentation patterns are driven by product stability.[32] In other words, in the example given above, Sn_{18}^+ dissociates to give $Sn_{11}^+ + Sn_7$ because these products are the lowest-energy products that can be generated from the Sn_{18}^+ parent cluster.

TABLE 2: Major Fragment Ions Observed in the Dissociation of $Cu_mSn_n^+$ Clusters

cluster	temperature range[a] °C	major fragment ions (in order of abundance)		
Sn_{10}	100−800	Sn_9		
$CuSn_{10}$	100−700	Sn_{10}	$CuSn_9$	
Sn_{11}	50−750	Sn_{10}		
$CuSn_{11}$	50	$CuSn_{10}$		
Cu_2Sn_{11}	600	$CuSn_{10}$		
Sn_{12}	50−500	Sn_{10}	Sn_6	
$CuSn_{12}$	100−400	$CuSn_{11}$	$CuSn_{10}$	
Cu_2Sn_{12}	700−800	$CuSn_{11}$	$CuSn_{10}$	
Sn_{13}	50−600	Sn_7	Sn_6	
$CuSn_{13}$	50−800	$CuSn_{12}$	$CuSn_{11}$	$CuSn_{10}$
Sn_{14}	50	Sn_7	Sn_6	Sn_8
$CuSn_{14}$	50	$CuSn_{10}$		
Cu_2Sn_{14}	500−800	Cu_2Sn_{13}	$CuSn_{10}$	Cu_2Sn_{12}
Sn_{15}	100−400	Sn_8	Sn_9	
$CuSn_{15}$	100−800	$CuSn_{11}$	$CuSn_{10}$	$CuSn_{14}$
Sn_{16}	50	Sn_9	Sn_{10}	Sn_8
$CuSn_{16}$	50	$CuSn_{10}$		
Sn_{17}	50	Sn_{10}	Sn_9	
$CuSn_{17}$	50	$CuSn_{10}$		
Cu_2Sn_{17}	600−800	Cu_2Sn_{16}	Cu_2Sn_{11}	$CuSn_{10}$
Cu_3Sn_{17}	600−800	Cu_3Sn_{16}	$CuSn_{11}$	
Cu_4Sn_{17}	850	Cu_4Sn_{16}		
Sn_{18}	100−500	Sn_{11}		
$CuSn_{18}$	100−500	$CuSn_{11}$	$CuSn_{10}$	
Cu_2Sn_{18}	300−500	Cu_2Sn_{11}		
Cu_3Sn_{18}	500−800	Cu_3Sn_{17}		
Cu_4Sn_{18}	800−850	Cu_4Sn_{17}	Cu_4Sn_{16}	
Sn_{19}	50−300	$CuSn_9$	Sn_{10}	Sn_{12}
$CuSn_{19}$	100−400	$CuSn_{12}$	$CuSn_{10}$	
Cu_2Sn_{19}	500−700	Cu_2Sn_{12}	Cu_2Sn_{13}	$CuSn_{10}$
Sn_{20}	100−300	Sn_{10}		
$CuSn_{20}$	50	$CuSn_{10}$		
Sn_{21}	50−300	Sn_{11}		
$CuSn_{21}$	50	$CuSn_{11}$		
$CuSn_{22}$	50	$CuSn_{15}$	$CuSn_{12}$	
Cu_2Sn_{22}	500−600	Cu_2Sn_{21}	Cu_2Sn_{16}	Cu_2Sn_{15}
Cu_3Sn_{22}	450−600	Cu_3Sn_{15}	Cu_3Sn_{16}	Cu_3Sn_{21}
Sn_{23}	100−400	Sn_{16}	Sn_{13}	
$CuSn_{23}$	100−300	$CuSn_{13}$	$CuSn_{10}$	$CuSn_{16}$

[a] Temperature range over which the dissociation processes were observed.

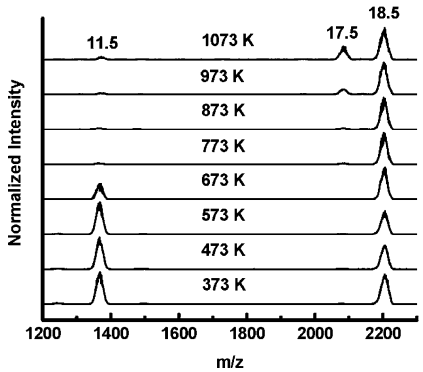

Figure 4. Fragmentation of the 18.5 half-integer peak as a function of the source extension temperature. All spectra were recorded with a collision cell injection energy of 350 eV. The intensities are normalized to the highest intensity peak within each spectrum. At low temperature, the 18.5 peak is $CuSn_{18}^+$, while at high temperature, it is $Cu_3Sn_{17}^+$.

Clusters with a single copper atom, $CuSn_n^+$, generally have similar fragmentation patterns to the pure tin clusters in that fission products dominate. An example of this is shown in Figure 4 which shows the fragmentation behavior of the 18.5 half-integer peak ($CuSn_{18}^+$) as a function of the source extension temperature. At close to room temperature, the main product is

$CuSn_{11}^+$. Inspection of Table 2 reveals that $CuSn_{11}^+$ and particularly $CuSn_{10}^+$ are very common products in the dissociation of the $CuSn_n^+$ clusters, which suggests that these clusters are particularly stable.

All the mass spectra in Figure 4 were recorded with a collision cell injection energy of 350 eV, so as the source extension temperature is raised, the amount of fragmentation is expected to systematically increase. At a temperature of 373 K, the main fragment is $CuSn_{11}^+$, but as the temperature is raised, this fragment apparently disappears. This occurs because the 18.5 peak changes from being $CuSn_{18}^+$ to $Cu_3Sn_{17}^+$ (a change that is accompanied by a shift in the peak position). $Cu_3Sn_{17}^+$ is more stable toward dissociation than $CuSn_{18}^+$, and so, it does not dissociate significantly until a much higher temperature is attained. The fragmentation pattern of $Cu_3Sn_{17}^+$ is significantly different from that of $CuSn_{18}^+$. Instead of generating the fission fragments characteristic of the pure tin clusters, $Cu_3Sn_{17}^+$ dissociates primarily by evaporating a tin atom to yield $Cu_3Sn_{16}^+$. This is a general result; as the tin clusters incorporate more copper atoms, they preferentially evaporate individual tin atoms rather than undergoing fission (see Table 2). Loss of a copper atom does occur, but this process is much less important than loss of a tin atom.

Discussion

Table 1 summarizes the range over which specific $Cu_mSn_n^+$ clusters are prominent in the mass spectra from the source. Although $CuSn_n^+$ can be observed with as few as seven tin atoms ($CuSn_7^+$), it first becomes prominent for $n = 10$. The $CuSn_n^+$ cluster persists up to $n = 15$, at which point the half-integer peak shifts to become predominantly $Cu_3Sn_{n-1}^+$. The $Cu_2Sn_{n-1}^+$ cluster becomes prominent at $n = 12$ and persists up to $n = 18$. $Cu_3Sn_{n-1}^+$ is prominent from $n = 15-21$. The smallest prominent clusters associated with a particular number of copper atoms are $CuSn_{10}^+$, $Cu_2Sn_{12}^+$, $Cu_3Sn_{15}^+$, $Cu_4Sn_{18}^+$, and $Cu_5Sn_{21}^+$. On the basis of DFT calculations, Kumar et al.[18] predicted $NiSn_{10}$ (which is isoelectronic with $CuSn_{10}^+$) to be particularly stable. The metal-encapsulated forms of $NiSn_{10}$ (there are several with similar energies) are predicted to be 2.2 eV lower in energy than Sn_{10} with the metal atom outside. This high stability presumably accounts for the prominence of the $CuSn_{10}^+$ cluster in the cluster mass spectra. $CuSn_{10}^+$ is also a dominant fragment ion in the dissociation of larger $Cu_mSn_n^+$ clusters, which provides further evidence that $CuSn_{10}^+$ is a particularly stable cluster. The isoelectronic CoM_{10}^- cluster has been found to be prominent for M = Ge, Sn, and Pb;[37] and $AlPb_{10}^+$ and $AlPb_{12}^+$ were found to be prominent in the mass spectra from laser vaporization of lead and aluminum in a two-rod source.[38] In the latter case, geometry optimization using density functional theory suggests that $AlPb_{12}^+$ is an icosahedron and that $AlPb_{10}^+$ is a bicapped tetragonal antiprism. Both structures have the aluminum atom encapsulated in the central position. The stability of these structures is attributed to favorable (close-packed) geometries coupled with optimally filled electronic shells. In other related work, $[Pt@Pb_{12}]^{2-}$ and $[Ni@Pb_{12}]^{2-}$ have been prepared in solution, and X-ray of their salts revealed a central metal atom encapsulated in a closo-$[Pb_{12}]^{2-}$ icosahedral Zintl ion and a closo-$[Pb_{10}]^{2-}$ bicapped square antiprism, respectively.[39,40] There is clearly a strong precedent for the formation of a stable, metal-encapsulated $CuSn_{10}^+$ cluster.

$Cu_mSn_n^+$ clusters with a particular number of copper atoms exist over a range of six or seven tin atoms. The largest prominent clusters for a particular number of copper atoms are $CuSn_{15}^+$, $Cu_2Sn_{18}^+$, $Cu_3Sn_{21}^+$, and presumably $Cu_4Sn_{24}^+$ and $Cu_5Sn_{27}^+$. These values correspond closely to the maximum cluster sizes found for $W_mSi_n^+$ clusters: WSi_{12}^+, $W_2Si_{18}^+$, $W_3Si_{22}^+$, $W_4Si_{26}^+$, and $W_5Si_{29}^+$. This sequence has been taken to indicate that the $W_mSi_n^+$ clusters adopt core−shell geometries. So, the observation that the $Cu_mSn_n^+$ clusters show a similar sequence raises the possibility that the copper-doped tin clusters generated by high-temperature annealing have core−shell geometries with a copper core surrounded by a tin shell. Note that the largest cluster sizes observed for the $Cu_mSn_n^+$ clusters are systematically smaller than for the $W_mSi_n^+$ clusters, which is expected because the Sn−Sn bond length is significantly longer than the Si−Si bond length. In the bulk, copper and tin form alloys, so it is noteworthy that, in the clusters studied here, a narrow range of compositions is favored. While $CuSn_n^+$ with n as small as 7 were observed in these studies, the $CuSn_n^+$ cluster really first becomes prominent at $n = 10$. As discussed above, $CuSn_{10}^+$ is a particularly stable cluster. Thus, if the annealed $Cu_mSn_n^+$ clusters do indeed adopt core−shell geometries, $CuSn_{10}^+$ (with a central copper atom) is probably the smallest. The main product observed in the dissociation of $CuSn_{10}^+$ is Sn_{10}^+, which might be thought to argue against a central copper atom. However, fragmentation is not a good probe of geometry, particularly if the cluster is strongly bound so that it can isomerize before dissociation. If indeed $CuSn_{10}^+$ has a core−shell structure, and a Sn_9 cage is too small to accommodate a Cu atom, the choice is between loss of the central atom to give the stable Sn_{10}^+ ion or loss of an atom from the shell to give $CuSn_9^+$; hence, loss of a copper atom may well be the preferred dissociation pathway. There is precedent for this behavior: Endohedral fullerenes appear to lose the metal atom when the cage gets too small.[41]

It is important to note that annealing does not just dissociate the weakly bound copper-doped tin clusters to leave behind the more stable ones. This does, however, appear to happen with the pure tin clusters: As the temperature is raised, only the strongly bound clusters survive, and the overall intensity drops substantially. For the copper-doped tin clusters, the clusters present at high temperatures have substantially different compositions than those present at low temperature, while the overall intensities have remained approximately the same. Thus, the copper-doped tin clusters seem to have incorporated more copper atoms during the annealing process. These additional copper atoms must come from free copper atoms in the buffer gas flow. There is presumably an activation barrier associated with the incorporation of more than one copper atom, which can be overcome by heating.

An interesting feature of the results presented here is the way the fission fragments vanish as the amount of copper in the cluster increases. Loss of individual atoms is the characteristic dissociation pathway of metal clusters, so it appears as though the copper atoms are "metalizing" the tin clusters. The fission fragments for pure tin clusters result because of the stability of the products. Thus, when $CuSn_{18}^+$ dissociates

$$CuSn_{18}^+ \rightarrow CuSn_{11}^+ + Sn_7$$

the fission fragments persist, because the $CuSn_{11}^+$ product is if anything more stable than the pure tin species (Sn_{11}^+). What then is responsible for the change in the dissociation pattern from fission to evaporation as the number of copper atoms increases? One possibility is that the presence of the copper destabilizes the fission products. Thus, when $Cu_3Sn_{17}^+$ dissociates by fission, it is not possible to find an energetically favorable location for all of the copper atoms. Sn_{17}^+ dissociates

to give mainly Sn_{10}^+ and Sn_7, and while $CuSn_{10}^+$ is a very stable species, there may not be a favorable location for the other two copper atoms. $Cu_3Sn_{10}^+$ and Cu_2Sn_7 do not appear to be very stable (on the basis of their absence in the cluster ion mass spectra). Hence, loss of a tin atom to give $Cu_3Sn_{16}^+$ may be the lowest-energy dissociation pathway of $Cu_3Sn_{17}^+$. An alternative explanation for the shift from fission to evaporation is that it reflects a change in the state of the dissociating cluster from solidlike (fission) to liquidlike (evaporation). The dissociation of pure tin clusters requires relatively low levels of excitation and occurs at a temperature below the clusters' melting temperatures.[42] Particularly prominent fission fragments such as Sn_{10}^+ are prominent because they are stable, and they are stable because they can adopt a favorable geometry. Clearly, the clusters must be in a solidlike state to realize this enhanced stability. On the other hand, for a liquid droplet, the preferred dissociation pathway is expected to be evaporation of individual atoms. Since increasing the amount of copper in the $Cu_mSn_n^+$ clusters increases the energy or temperature required to cause dissociation, it is possible that the clusters with a larger number of copper atoms melt before they dissociate. Thus, the shift from fission to evaporation with an increasing number of copper atoms may reflect a change from dissociation from a solidlike phase to dissociation from a liquidlike phase.

Acknowledgment. We gratefully acknowledge the support of the National Science Foundation. We thank Dr. Vijay Kumar for helpful comments.

References and Notes

(1) Jackson, K.; Nellemore, B. *Chem. Phys. Lett.* **1996**, *254*, 249−256.
(2) Hagelberg, F.; Yanov, I.; Leszczynski, J. *THEOCHEM* **1999**, *487*, 183−192.
(3) Kumar, V.; Kawazoe, Y. *Phys. Rev. Lett.* **2001**, *87*, 045503.
(4) Kumar, V.; Kawazoe, Y. *Phys. Rev. B* **2002**, *65*, 073404.
(5) Xiao, C.; Abraham, A.; Quinn, R.; Hagelberg, F.; Lester, W. A. *J. Phys. Chem. A* **2002**, *106*, 11380−11393.
(6) Pacheco, J. M.; Gueorguiev, G. K.; Martins, J. L. *Phys. Rev. B* **2002**, *66*, 033401.
(7) Xiao, C.; Hagelberg, F.; Lester, W. A. *Phys. Rev. B* **2002**, *66*, 075425.
(8) Kumar, V.; Majumder, C.; Kawazoe, Y. *Chem. Phys. Lett.* **2002**, *363*, 319−322.
(9) Khanna, S. N.; Rao, B. K.; Jena, P.; Nayak, S. K. *Chem. Phys. Lett.* **2003**, *373*, 433−438.
(10) Lu, J.; Nagase, S. *Chem. Phys. Lett.* **2003**, *372*, 394−398.
(11) Kumar, V.; Kawazoe, Y. *Appl. Phys. Lett.* **2003**, *83*, 2677−2679.
(12) Hagelberg, F.; Xiao, C.; Lester, W. A. *Phys. Rev. B* **2003**, *67*, 035426.
(13) Lu, J.; Nagase, S. *Phys. Rev. Lett.* **2003**, *90*, 115506.
(14) Kumar, V. *Eur. Phys. J. D* **2003**, *24*, 227−232.
(15) Miyazaki, T.; Hiura, H.; Kanayama, T. *Eur. Phys. J. D* **2003**, *24*, 241−244.
(16) Sen, P.; Mitas, L. *Phys. Rev. B* **2003**, *68*, 155404.
(17) Huda, M. N.; Ray, A. K. *Phys. Rev. A* **2004**, *69*, 011201.
(18) Kumar, V.; Singh, A. K.; Kawazoe, Y. *Nano Lett.* **2004**, *4*, 677−681.
(19) Kawamura, H.; Kumar, V.; Kawazoe, Y. *Phys. Rev. B* **2004**, *70*, 193402.
(20) Majumder, C.; Kulshreshtha, S. K. *Phys. Rev. B* **2004**, *70*, 245426.
(21) Kawamura, H.; Kumar, V.; Kawazoe, Y. *Phys. Rev. B* **2004**, *70*, 245433.
(22) Beck, S. M. *J. Chem. Phys.* **1987**, *87*, 4233−4234.
(23) Beck, S. M. *J. Chem. Phys.* **1989**, *90*, 6306−6312.
(24) Ohara, M.; Miyajima, K.; Pramann, A.; Nakajima, A.; Kaya, K. *J. Phys. Chem. A* **2002**, *106*, 3702−3705.
(25) Ohara, M.; Koyasu, K.; Kakajima, A.; Kaya, K. *Chem. Phys. Lett.* **2003**, *371*, 490−497.
(26) Ferhati, A.; McMahon, T. B.; Ohanessian, G. *J. Am. Chem. Soc.* **1996**, *118*, 5997−6009.
(27) Hiura, H.; Miyazaki, T.; Kanayama, T. *Phys. Rev. Lett.* **2001**, *86*, 1733−1736.
(28) Negishi, A.; Kariya, N.; Sugawara, K.; Arai, I.; Hiura, H.; Kanayama, T. *Chem. Phys. Lett.* **2004**, *388*, 463−467.
(29) Shvartsburg, A. A.; Jarrold, M. F. *Phys. Rev. A* **1999**, *60*, 1235−1239.
(30) Shvartsburg, A. A.; Jarrold, M. F. *Chem. Phys. Lett.* **2000**, *317*, 615−618.
(31) Joshi, K.; Kanhere, D. G.; Blundell, S. A. *Phys. Rev. B* **2003**, *67*, 235413.
(32) Joshi, K.; Kanhere, D. G.; Blundell, S. A. *Phys. Rev. B* **2002**, *66*, 155329.
(33) Chuang, F.-C.; Wang, C. Z.; Öğüt, S.; Chelikowsky, J. R.; Ho, K. M. *Phys. Rev. B* **2004**, *69*, 165408.
(34) Tai, Y.; Murakami, J.; Marumder, C.; Kumar, V.; Mizuseki, H.; Kawazoe, Y. *J. Chem. Phys.* **2002**, *117*, 4317−4322.
(35) Breaux, G. A.; Benirschke, R. C.; Sugai, T.; Kinnear, B. S.; Jarrold, M. F. *Phys. Rev. Lett.* **2003**, *91*, 215508.
(36) Jarrold, M. F.; Honea, E. C. *J. Phys. Chem.* **1991**, *95*, 9181−9185.
(37) Zhang, X.; Li, G.; Xing, X.; Zhao, X.; Tang, Z.; Gao, Z. *Rapid Commun. Mass Spectrom.* **2001**, *15*, 2399−2403.
(38) Neukermans, S.; Janssens, E.; Chen, Z. F.; Silverans, R. E.; Schleyer, P. v. R.; Lievens, P. *Phys. Rev. Lett.* **2004**, *92*, 163401.
(39) Esenturk, E. N.; Fettinger, J.; Lam, Y.-F.; Eichhorn, B. *Angew. Chem. Int. Ed.* **2004**, *43*, 2132−2134.
(40) Esenturk, E. N.; Fettinger, J.; Eichhorn, B. *Chem. Commun.* **2005**, 247−249.
(41) Weiss, F. D.; Elkind, J. L.; O'Brien, S. C.; Curl, R. F.; Smalley, R. E. *J. Am. Chem. Soc.* **1988**, *110*, 4464−4465.
(42) Breaux, G. A.; Neal, C. M.; Cao, B.; Jarrold, M. F. *Phys. Rev. B* **2005**, *71*, 073410.